Agricultural and Forest Meteorology 213 (2015) 240–250

Contents lists available at ScienceDirect

Agricultural and Forest Meteorology

journal homepage: www.elsevier.com/locate/agrformet

Effects of in-situ and reanalysis climate data on estimation of cropland gross primary production using the Vegetation Photosynthesis Model

Cui Jin[a], Xiangming Xiao[a,b,*], Pradeep Wagle[a], Timothy Griffis[c], Jinwei Dong[a], Chaoyang Wu[d], Yuanwei Qin[a], David R. Cook[e]

[a] Department of Microbiology and Plant Biology, and Center for Spatial Analysis, University of Oklahoma, Norman, OK 73019, USA
[b] Institute of Biodiversity Sciences, Fudan University, Shanghai 200433, China
[c] Department of Soil, Water and Climate, University of Minnesota, St. Paul, MN 55108, USA
[d] Institute of Remote Sensing and Digital Earth, Chinese Academy of Sciences, Beijing 100101, China
[e] Argonne National Laboratory, Environmental Science Division, Lemont, IL 60439, USA

ARTICLE INFO

Article history:
Received 3 January 2015
Received in revised form 27 May 2015
Accepted 6 July 2015

Keywords:
Vegetation Photosynthesis Model (VPM)
NARR
MODIS
AmeriFlux
Downward shortwave radiation
Vegetation indices

ABSTRACT

Satellite-based Production Efficiency Models (PEMs) often require meteorological reanalysis data such as the North America Regional Reanalysis (NARR) by the National Centers for Environmental Prediction (NCEP) as model inputs to simulate Gross Primary Production (GPP) at regional and global scales. This study first evaluated the accuracies of air temperature (T_{NARR}) and downward shortwave radiation (R_{NARR}) of the NARR by comparing with in-situ meteorological measurements at 37 AmeriFlux non-crop eddy flux sites, then used one PEM – the Vegetation Photosynthesis Model (VPM) to simulate 8-day mean GPP (GPP_{VPM}) at seven AmeriFlux crop sites, and investigated the uncertainties in GPP_{VPM} from climate inputs as compared with eddy covariance-based GPP (GPP_{EC}). Results showed that T_{NARR} agreed well with in-situ measurements; R_{NARR}, however, was positively biased. An empirical linear correction was applied to R_{NARR}, and significantly reduced the relative error of R_{NARR} by ~25% for crop site-years. Overall, GPP_{VPM} calculated from the in-situ ($GPP_{VPM(EC)}$), original ($GPP_{VPM(NARR)}$) and adjusted NARR ($GPP_{VPM(adjNARR)}$) climate data tracked the seasonality of GPP_{EC} well, albeit with different degrees of biases. $GPP_{VPM(EC)}$ showed a good match with GPP_{EC} for maize (*Zea mays* L.), but was slightly underestimated for soybean (*Glycine max* L.). Replacing the in-situ climate data with the NARR resulted in a significant overestimation of $GPP_{VPM(NARR)}$ (18.4/29.6% for irrigated/rainfed maize and 12.7/12.5% for irrigated/rainfed soybean). $GPP_{VPM(adjNARR)}$ showed a good agreement with $GPP_{VPM(EC)}$ for both crops due to the reduction in the bias of R_{NARR}. The results imply that the bias of R_{NARR} introduced significant uncertainties into the PEM-based GPP estimates, suggesting that more accurate surface radiation datasets are needed to estimate primary production of terrestrial ecosystems at regional and global scales.

1. Introduction

Croplands cover 12% of the global ice-free terrestrial surface (Ramankutty et al., 2008) and provide food for more than seven billion people in the world. Increasing demand for food under the changing climate is one of the great challenges in the coming decades (Guanter et al., 2014; Lobell and Asner, 2003). Gross Primary Production (GPP) of croplands is the total carbon uptake through photosynthesis. A recent modeling study estimated that croplands have an annual sum of 11 Pg C yr^{-1} GPP, accounting for ~10% of the global terrestrial GPP (Chen et al., 2014). Crop cultivation and production vary substantially over space and time. Thus, an accurate quantification of cropland GPP is critical for global food security (Wheeler and von Braun, 2013), biofuel production (Landis et al., 2008), and understanding variations in the terrestrial carbon cycle (Haberl et al., 2007).

Production Efficiency Models (PEMs) have been widely used to quantify the spatial-temporal GPP variations of terrestrial ecosystems using the satellite and climate data as inputs. The PEMs, originating from Monteith's theoretical concept about light use efficiency (LUE) (Monteith, 1972; Monteith and Moss, 1977), estimate GPP as the product of the photosynthetically active radiation (PAR, MJ m^{-2}), the fraction of PAR absorbed by the vegetation

* Corresponding author at: 101 David L. Boren Blvd., Norman, OK 73019-5300, USA.
E-mail address: xiangming.xiao@ou.edu (X. Xiao).

http://dx.doi.org/10.1016/j.agrformet.2015.07.003
0168-1923/

(fPAR), and the conversion efficiency of absorbed PAR for carbon fixation (ε, g C MJ^{-1}) (GPP = $\varepsilon \times$ fPAR $\times$ PAR). The PEMs for croplands can be classified into two categories based on fPAR and ε estimation methods. The first category calculates fPAR and ε separately. This approach has been applied in the Global Production Efficiency Model (GLO-PEM) (Prince and Goward, 1995), the MODIS Daily Photosynthesis model (MODIS-PSN) (Running et al., 2000), the C-Fix model (Veroustraete et al., 2002), and the Vegetation Photosynthesis Model (VPM) (Xiao et al., 2004a,b). The second type of PEMs, referred as the Greenness and Radiation (GR) model, uses the chlorophyll-related vegetation indices (VI_{chl}) as a proxy of $\varepsilon \times$ fPAR (GPP $\propto VI_{chl} \times$ PAR) (Gitelson et al., 2006; Peng and Gitelson, 2011, 2012; Peng et al., 2011; Wu et al., 2009; Zhang et al., 2014, 2015).

Challenges remain, however, in applying PEMs due to model structure and model inputs. Several attempts have been made to address the uncertainties from the PEM algorithm itself, including the assumption of linear response of photosynthesis to light intensity (Chen et al., 1999), constant maximum LUE for one ecosystem (Heinsch et al., 2006), the impacts of diffuse radiation (He et al., 2013; Zhang et al., 2012), and the incomplete integration of environmental regulations (temperature, water, phenology, etc.) to photosynthetic processes (Dong et al., 2015; Yuan et al., 2014). Most uncertainty analyses overlooked the potential impacts of model inputs on the application of PEMs to regional or global primary production monitoring.

Meteorological reanalysis data produces continuous and near real-time climate monitoring via data assimilation models, and has been the major climate input of PEMs for the large-scale primary production simulation (Feng et al., 2007; Running et al., 2004; Xiao et al., 2011; Yuan et al., 2010). Studies have reported that the meteorological reanalysis data can be spatially and temporally biased from the ground observations, in particular for downward shortwave radiation when estimating PAR (Babst et al., 2008; Cai et al., 2014; Decker et al., 2012; Troy and Wood, 2009; Zhang et al., 2007; Zhao et al., 2006, 2013a; Zib et al., 2012). PEMs have been found very sensitive to the accuracy of climate reanalysis variables (Cai et al., 2014; Heinsch et al., 2006; Zhang et al., 2007; Zhao et al., 2006). For example, Heinsch et al. (2006) reported that the errors associated with the standard MODIS GPP product were mainly attributed to the NASA's Data Assimilation Office (DAO) reanalysis data. Previous sensitivity analyses of PEMs to climate inputs focused on global reanalysis data, the spatial resolution of which is too coarse to delineate the local climatic variations.

The North America Regional Reanalysis (NARR) by the National Centers for Environmental Prediction (NCEP) is the only currently available long-term regional reanalysis data. Compared with the NCEP global reanalysis datasets, the NARR substantially improves the spatio-temporal resolutions along with the accuracy of climate variables (Mesinger et al., 2006) and could be an alternative climate driver of regional GPP estimates in particular for croplands, one of the most heterogeneous landscapes. There has been very limited research regarding the uncertainties of PEMs in relation to the NARR. Therefore, careful investigation of the accuracy of the NARR and its impacts on cropland GPP estimates at site level is an indispensable step prior to the large scale application of these tools.

The objectives of this study were to: (1) evaluate the accuracy of the NARR (air temperature and downward shortwave radiation) as compared to the in-situ observations from the AmeriFlux network at 8-day intervals; (2) adjust the NARR based on the statistical differences from in-situ meteorological measurements; and (3) quantify the impacts of different climate inputs (in-situ meteorological data and the original and adjusted NARR data) on the GPP simulation for maize and soybean using the VPM at seven AmeriFlux crop sites (40 site-years).

2. Data and methods

2.1. NARR

The NARR is produced at a spatial resolution of 32 km and a temporal resolution of 3-h. We obtained the NARR daily gridded air temperature (T_{NARR}) and downward shortwave radiation (R_{NARR}) from http://www.esrl.noaa.gov/psd/. The daily T_{NARR} and R_{NARR} for the pixels covering AmeriFlux sites were extracted for the available site-years at 44 AmeriFlux sites and were aggregated to 8-day intervals to match the temporal resolution of MODIS products.

2.2. MODIS land surface reflectance, vegetation indices products

This study used the 8-day 500 m MODIS Surface Reflectance product – MOD09A1 to derive vegetation indices. The time-series MOD09A1 data for the crop sites were extracted from the MODIS data portal at the Earth Observation and Modeling Facility (EOMF), University of Oklahoma (http://www.eomf.ou.edu/visualization/manual/). The Enhanced Vegetation Index (EVI) and Land Surface Water Index (LSWI) were calculated for every 8-day observation using Eqs. (1) and (2).

$$EVI = 2.5 \times \frac{\rho_{NIR_1} - \rho_{red}}{\rho_{NIR_1} + 6 \times \rho_{red} - 7.5 \times \rho_{blue} + 1} \quad (1)$$

$$LSWI = \frac{\rho_{NIR_1} - \rho_{SWIR_1}}{\rho_{NIR_1} + \rho_{SWIR_1}} \quad (2)$$

where ρ_{NIR_1}, ρ_{red}, ρ_{blue}, and ρ_{SWIR_1} are the MOD09A1 surface reflectance for NIR_1 (841-876 nm), red (620–670 nm), blue (459–479 nm), and $SWIR_1$ (1628–1652 nm), respectively. A two-step gap-filling procedure was applied to gap-fill bad-quality observations within the time series of vegetation indices (Xiao et al., 2004a,b).

2.3. In-situ meteorological observations and CO_2 flux data

The AmeriFlux network consists of eddy covariance flux sites for monitoring the long-term ecosystem-scale exchange of carbon, energy, and water in North America (Baldocchi et al., 2001). Meteorological observations such as temperature, precipitation, and radiation are also collected at these sites.

We obtained all available 8-day Level 4 data of the AmeriFlux sites covering the conterminous U.S. from http://ameriflux.lbl.gov/Pages/default.aspx (Fig. 1). The Level 4 data included air temperature (T_{EC}), downward shortwave radiation (R_{EC}), and CO_2 flux data. This study used the standardized GPP (GPP_{EC}), which was partitioned from net ecosystem CO_2 exchange (NEE). By screening quality flags, only the most reliable observations were chosen for analysis. T_{EC} and R_{EC} from 37 non-crop sites (139 site-years) were used to evaluate and to adjust the NARR, if there were large biases. A total of 23 site-years of T_{EC} and R_{EC} and 40 site-years of GPP_{EC} from seven crop sites were used to validate the adjusted NARR and to evaluate the VPM-simulated GPP, respectively (Table 1). The crop sites were located in the Midwest U.S. corn and soybean belt, and were under different agricultural management practices. US-NE1 was a continuous irrigated maize site and US-NE2 was an irrigated maize/soybean rotation site. The other five sites were rainfed maize/soybean rotation sites. The detailed descriptions about these sites can be found in site specific publications (Griffis et al., 2005; Meyers and Hollinger, 2004; Verma et al., 2005).

It is important to mention that a direct comparison between the in-situ AmeriFlux observations and the NARR data without considering the differences of spatial scales might introduce some uncertainties. The in-situ observations can be affected by local environment conditions (terrain, hydrology, land cover etc.), while the

Table 1
A summary description of the AmeriFlux eddy flux crop sites.

Site ID	Latitude	Longitude	Years of T_{EC}[a], R_{EC}[b]	Crop type	Years of GPP_{EC}[c]
US-NE1	−96.4766	41.165	2002–2012	Irrigated maize	2002–2005, 2007–2012
US-NE2	−96.4701	41.1649	2001–2012	Irrigated maize	2001, 2003, 2005, 2007, 2009–2012
				Irrigated soybean	2002, 2004, 2006, 2008
US-NE3	−96.4396	41.1797	2001–2012	Rainfed maize	2001, 2003, 2005, 2009, 2011
				Rainfed soybean	2002, 2004, 2008, 2010
US-RO1	−93.0898	44.7143	2004–2006	Rainfed maize	2005
				Rainfed soybean	2006
US-RO3	−93.0893	44.7217	2004–2006	Rainfed maize	2005
US-IB1	−88.2904	40.0062	2006–2007	Rainfed maize	2006
				Rainfed soybean	2007
US-Bo1	−88.2227	41.8593	2001–2006	Rainfed maize	2005
				Rainfed soybean	2002, 2004, 2006

[a] and [b]Air temperature and downward shortwave radiation observed from the AmeriFlux eddy flux sites.
[c]8-day Level-4 GPP estimates from the AmeriFlux eddy flux sites.

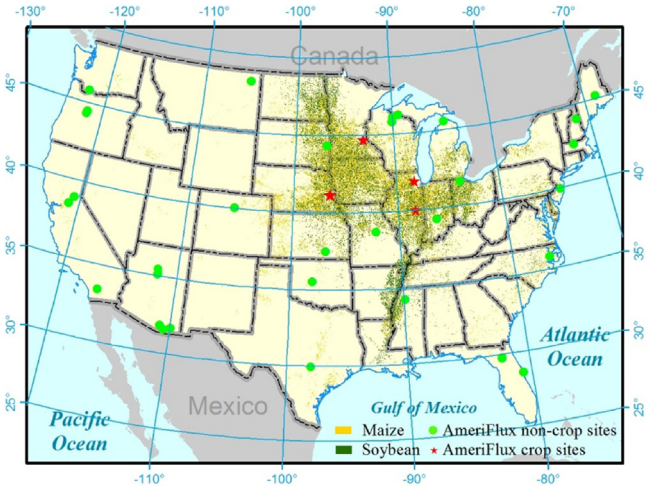

Fig. 1. Location of the AmeriFlux eddy flux sites. Circles denote the non-crop sites for accuracy assessment of the NARR and stars denote the crop sites used to evaluate the VPM-based GPP estimates. The base map is the 2013 Cropland Data Layer (CDL) from the National Agricultural Statistics Service (NASS).

NARR might be too coarse to delineate local environment variations. However, the AmeriFlux is currently the best available dataset providing high-quality and synchronized observation of radiation, temperature, water and carbon fluxes under standard protocols.

2.4. The Vegetation Photosynthesis Model (VPM)

The VPM is one PEM based on the conceptual partition of the light absorption by chlorophyll pigments and nonphotosynthetic vegetation (NPV such as branches, trunks, or senescent leaves) (Xiao et al., 2004a,b). The VPM defines the fPAR as the fraction of PAR absorbed by plant chlorophyll ($fPAR_{chl}$):

$$GPP = \varepsilon \times fPAR_{chl} \times PAR \quad (3)$$

$$fPAR_{chl} = EVI \quad (4)$$

$$\varepsilon = \varepsilon_0 \times T_{scalar} \times W_{scalar} \quad (5)$$

where PAR is calculated as $0.45 \times R$ (R, downward shortwave solar radiation); $fPAR_{chl}$ is equivalent to EVI; Light use efficiency, ε, is estimated as a function of the maximum light use efficiency (ε_0), temperature (T_{scalar}) and water condition (W_{scalar}). The ε_0 values of 3.12 g C MJ^{-1} for maize (Kalfas et al., 2011) and 1.75 g C MJ^{-1} for soybean (Wagle et al., 2015) were used in this study.

The effect of temperature scalar (T_{scalar}) on GPP is calculated using the equation from the Terrestrial Ecosystem Model (Raich et al., 1991):

$$T_{scalar} = \begin{cases} \dfrac{(T - T_{min})(T - T_{max})}{[(T - T_{min})(T - T_{max})] - (T - T_{opt})^2}, & T_{min} \le T \le T_{max} \\ 0, & T \le T_{min},\ T \ge T_{max} \end{cases} \quad (6)$$

where T is 8-day mean air temperature; T_{min}, T_{opt}, and T_{max} are minimum, optimum, and maximum temperatures for vegetation photosynthesis, respectively, and were set to 10 °C, 28 °C, 48 °C for maize (Kalfas et al., 2011), and −1 °C, 28 °C, 50 °C for soybean (Wagle et al., 2015).

The effect of water scalar (W_{scalar}) on GPP is calculated with LSWI:

$$W_{scalar} = \begin{cases} \dfrac{1 + LSWI}{1 + LSWI_{max}}, & LSWI > 0 \\ LSWI + LSWI_{max}, & LSWI \le 0 \end{cases} \quad (7)$$

where $LSWI_{max}$ is the maximum LSWI during growing season.

This study used the VPM to simulate three sets of GPP_{VPM}: $GPP_{VPM(EC)}$, $GPP_{VPM(NARR)}$, and $GPP_{VPM(adjNARR)}$, using T and R from eddy flux sites (T_{EC}, R_{EC}), the NARR (T_{NARR}, R_{NARR}), and the adjusted NARR (T_{NARR}, $R_{adjNARR}$), respectively.

2.5. Statistical analysis

To quantify the differences between T_{NARR} and T_{EC}, R_{NARR} and R_{EC}, correlation coefficient (ρ), ratio of standard deviation (σ_{ratio}), bias, and root-mean-square-error (RMSE) were calculated for each non-crop site-year. The histogram of each statistics was summarized for all non-crop site-years to characterize the overall accuracy of T_{NARR} and R_{NARR}.

Mean squared error (MSE) was calculated for T_{NARR} and R_{NARR} of each site-year, and decomposed into three terms (Decker et al., 2012; Gupta et al., 2009), such that

$$MSE = 2\sigma_{NARR}\sigma_{EC}(1 - \rho) + (\sigma_{NARR} - \sigma_{EC})^2 + (\mu_{NARR} - \mu_{EC})^2 \quad (8)$$

where μ_{EC} and σ_{EC} are the mean and standard deviation for the in-situ observations, respectively. μ_{NARR} and σ_{NARR} are the mean and standard deviation for the NARR, respectively. The first, second, and third terms in Eq. (8) were represented in ternary diagrams to concisely visualized the contribution of correlation (ρ), consistency of variation (σ_{ratio}), and bias (bias and RMSE) to the overall disagreements between T_{NARR} and T_{EC} and between R_{NARR} and R_{EC}.

The simple linear regression between R_{EC} and R_{NARR} was also calculated for all non-crop site-years ($R_{EC} = \alpha \times R_{NARR}$). On the basis of the spatial pattern of regression coefficients (α), an empirical ratio-based adjustment was applied to R_{NARR} at the crop sites ($R_{adjNARR}$).

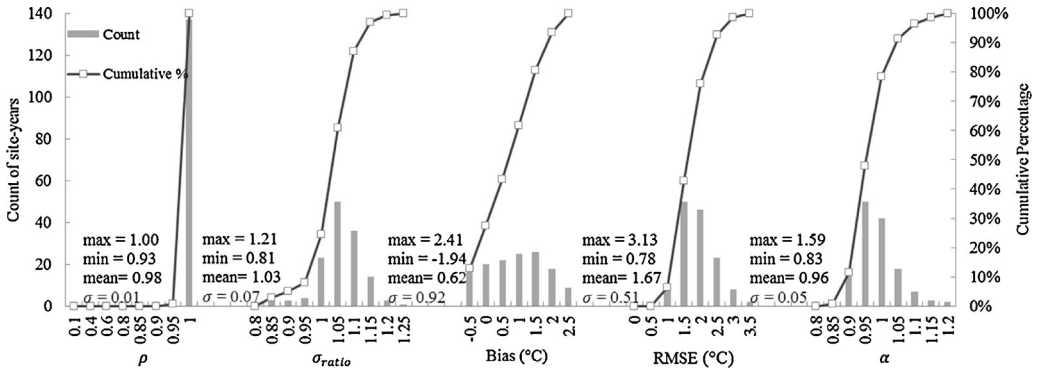

Fig. 2. Distribution histograms of correlation coefficient (ρ), ratio of standard deviation (σ_{ratio}), bias, root-mean-square-error (RMSE), and regression coefficient (α) for 8-day air temperature from AmeriFlux (T_{EC}) and NARR (T_{NARR}) across the non-crop site-years.

Relative error (RE), RMSE, regression coefficient (α), and coefficient of determination (R^2) of the simple linear regression between R_{NARR} and R_{EC}, and $R_{adjNARR}$ and R_{EC} were obtained to quantify the adjustment performance.

This study implemented a top-down strategy to evaluate the impact of different climate inputs on GPP_{VPM}. First, the statistics factors described above were used to quantify how $GPP_{VPM(EC)}$, $GPP_{VPM(NARR)}$, and $GPP_{VPM(adjNARR)}$ matched GPP_{EC} for individual crops. Second, the similarities between GPP_{VPM} and GPP_{EC} across individual crop-sites were evaluated using Taylor diagrams. Taylor diagrams provide a statistical summary of the similarity of variability pattern (ρ), the agreement of the variability amplitudes (represented by the ratio of normalized standard deviation, $\bar{\sigma}_{ratio}$), and the centered RMSE between the modeled results and the observations (Gleckler et al., 2008; Taylor, 2001). In addition, annual mean RMSE of GPP_{VPM} was calculated for each crop site-year.

3. Results

3.1. Comparison of air temperature

T_{NARR} agreed well with T_{EC} for almost all non-crop site-years. T_{NARR} was significantly correlated with T_{EC} ($\rho > 0.95$ for 139 site-years, Fig. 2). In addition, T_{NARR} showed a similar amplitude of variation as in T_{EC}, as ~82% of site-years had σ_{ratio} within ±10% error. T_{NARR} was mostly overestimated with a positive bias of 0.5–2.5 °C and a mean RMSE of 1.67 °C. The simple linear regression confirmed the good agreement between T_{NARR} and T_{EC}. T_{NARR} showed a strong linear regression with T_{EC} (α across 129 site-years was in a range of 1 ± 0.1, $R^2 > 0.95$, $p < 0.001$). MSE was determined by both the bias and correlation, as the contribution of bias and correlation was over 0.8 at 86% of the site-years (Fig. 3).

T_{NARR} was also relatively accurate at the crop sites. The simple linear regression indicated that T_{NARR} agreed well with T_{EC} for all crop site-years ($\alpha = 1.04$, RE = 11.6%, RMSE = 1.4 °C, $R^2 = 0.99$, Fig. 4). T_{NARR} accounted for over 98% of the seasonal dynamics of T_{EC} for individual crop sites on annual scale (Table 2). α varied from 1.0 to 1.1 among the crop sites. RE and RMSE were −1.4% to 7.3% and 1.2–1.7 °C, respectively. Considering the relatively high accuracy at non-crop and crop site-years, the 8-day T_{NARR} was used as the VPM input without any correction.

3.2. Comparison of downward shortwave radiation

R_{NARR} was well correlated with R_{EC} ($\rho > 0.9$ at 94% of the non-crop site-years, Fig. 5). However, it was overestimated with $\sigma_{ratio} > 1.1$ at 67% of the site-years. The bias was positive across all site-years on an average of 3.55 MJ m^{-2} day^{-1}. 60% of the site-years had a RMSE of 3–5 MJ m^{-2} day^{-1}. The bias was the dominant

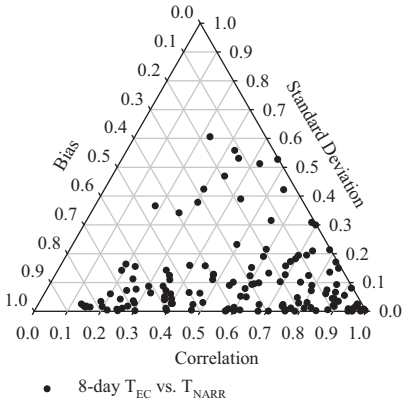

Fig. 3. Contributions of correlation (ρ), consistency of variation (σ_{ratio}), and bias to the mean squared error (MSE) for the 8-day NARR air temperature (T_{NARR}) across the non-crop site-years.

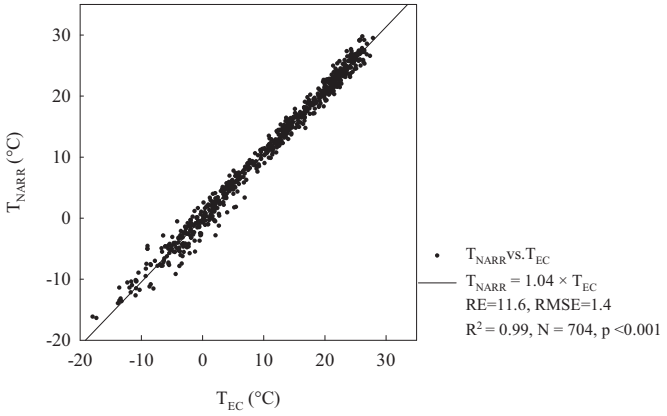

Fig. 4. Comparisons of 8-day air temperature between AmeriFlux (T_{EC}) and NARR (T_{NARR}) across all crop site-years.

contributor to MSE (Fig. 6). The contribution of bias was >0.5 at 133 of 139 site-years, indicating the disagreement between R_{NARR} and R_{EC} was systematic.

R_{NARR} showed a significant linear regression with R_{EC} at each non-crop site-year (Fig. 5). However, α was quite variable (0.63–0.95). α slightly decreased with the latitude increasing or the longitude decreasing (Fig. 7). α was more stable within the longitude range of 85–100 °W than it was across 40–47.5 °N for the region covering the crop sites (Fig. 7 highlighted in gray). Thus, the median of α values (0.81) within the longitude of 85–100 °W was used as a ratio to adjust the bias of R_{NARR} at the crop sites.

Table 2
Statistics of the comparison of the 8-day NARR air temperature, original, and adjusted downward shortwave radiation with the AmeriFlux observations for the individual crop sites.

Site ID	T_{EC}[a] vs. T_{NARR}[b]				R_{EC}[c] vs. R_{NARR}[d]			R_{EC} vs. $R_{adjNARR}$[e]			
	RE	RMSE	α	R^2	RE	RMSE	α	R^2	RE	RMSE	α
US-NE1/2/3	7.3 ± 5.9	1.7 ± 0.55	1.1 ± 0.04	0.98	21.8 ± 2.6	3.9 ± 0.4	1.2 ± 0.03	0.9 ± 0.03	−2.5 ± 2.1	1.6 ± 0.02	0.97 ± 0.02
US-RO1/3	−1.4 ± 5.2	1.6 ± 0.33	1.0 ± 0.01	0.99 ± 0.01	26.5 ± 2.2	4.2 ± 0.2	1.2 ± 0.02	0.91 ± 0.03	1.2 ± 1.8	1.6 ± 0.22	0.99 ± 0.02
US-IB1	4.6 ± 0.1	1.3 ± 0.12	1.1 ± 0.02	0.99	28.6 ± 1.5	4.9 ± 0.26	1.3	0.89 ± 0.05	2.9 ± 1.2	1.8 ± 0.23	1.01
US-Bo1	7.1 ± 2.0	1.2 ± 0.17	1.0 ± 0.01	0.99	22.7 ± 7.6	3.8 ± 0.78	1.2 ± 0.08	0.9 ± 0.05	−1.9 ± 6.1	2.0 ± 0.40	0.96 ± 0.06

[a] and [b]Air temperature of the AmeriFlux and NARR data (°C).
[c–e]Downward shortwave radiation of the AmeriFlux, the NARR before and after adjustment (MJ m^{-2} day^{-1}).

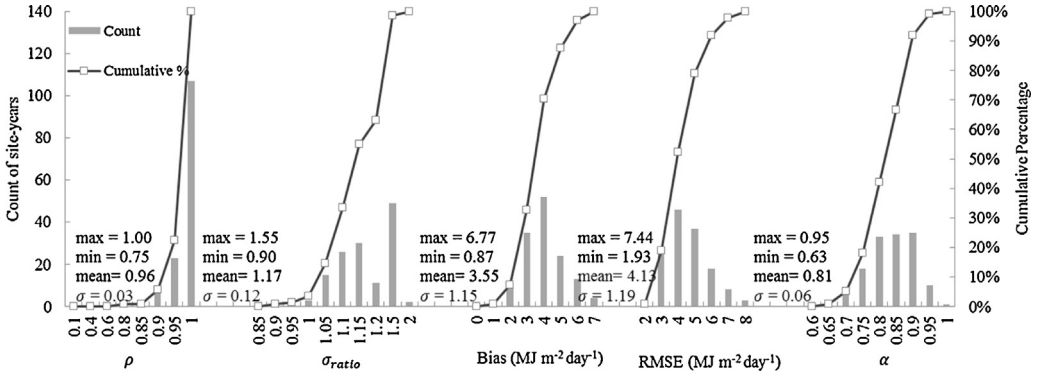

Fig. 5. Distribution histograms of correlation coefficient (ρ), ratio of standard deviation (σ_{ratio}), bias, root-mean-square-error (RMSE), and regression coefficient (α) for 8-day downward shortwave radiation between AmeriFlux (R_{EC}) and NARR (R_{NARR}) across the non-crop site-years.

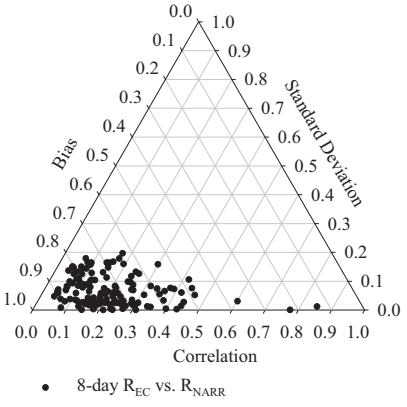

Fig. 6. Contributions of correlation (ρ), consistency of variation (σ_{ratio}), and bias to the Mean Squared Error (MSE) for the 8-day NARR downward shortwave radiation (R_{NARR}) across the non-crop site-years.

The adjustment substantially reduced the bias of R_{NARR} at the crop sites (Fig. 8). R_{NARR} was overestimated by 28.2% on average. $R_{adjNARR}$ evenly distributed along 1:1 line and RMSE was reduced to 1.7 MJ^{-2} day^{-1}.

R_{NARR} explained ~90% of the variations of R_{EC} across each crop site (Table 2). Similar to the non-crop sites, R_{NARR} was strongly overestimated (RE > 22%) at the crop sites. The annual RMSE varied from 3.8 MJ m^{-2} day^{-1} to 4.9 MJ m^{-2} day^{-1}. After the adjustment, α was close to 1, and RE and RMSE of $R_{adjNARR}$ decreased to −2.5% to 3% and 1.6–2 MJ m^{-2} day^{-1}, respectively.

3.3. Comparison of VPM-based (GPP_{VPM}) and the flux tower-based (GPP_{EC}) estimates

The seasonal dynamics of $GPP_{VPM(EC)}$, $GPP_{VPM(NARR)}$, and $GPP_{VPM(adjNARR)}$ corresponded well with GPP_{EC} for both maize and soybean (Fig. 9). At the leaf-on stage during late-May to June, GPP_{EC} started to exceed 1 g C m^{-2} day^{-1} and GPP_{VPM} also rose rapidly,

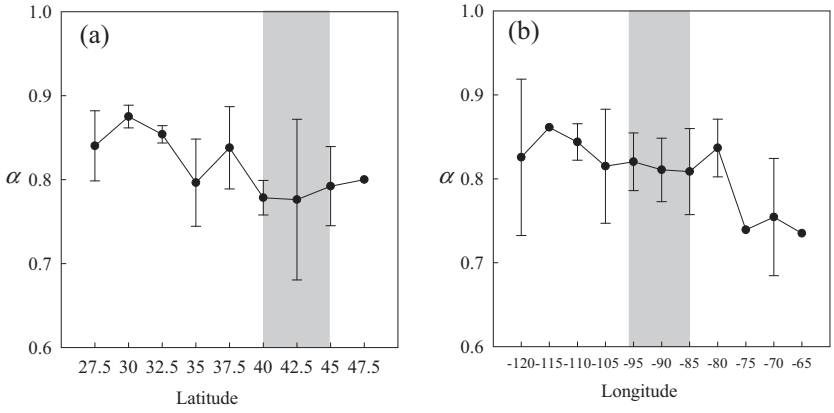

Fig. 7. Spatial patterns of regression coefficient (α) between 8-day downward shortwave radiation from AmeriFlux (R_{EC}) and NARR (R_{NARR}), with geographical distribution of crop sites highlighted: (a) α averaged along the 2.5° latitude gradient and (b) α averaged along the 5° longitude gradient.

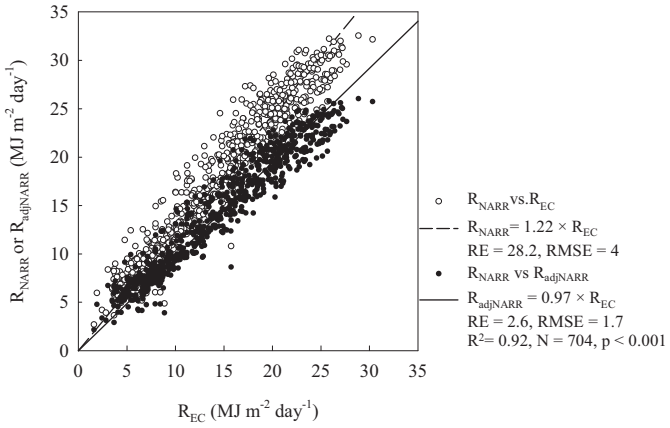

Fig. 8. Comparisons of 8-day downward shortwave radiation between AmeriFlux (R_{EC}) and the NARR before and after adjustment (R_{NARR}, $R_{adjNARR}$) for all crop site-years.

and both reached a maximum at the peak growing season during late-July to early-August. After the crops matured and approached the harvest date in September, both GPP_{EC} and GPP_{VPM} began to decrease and were lower than 1 g C m^{-2} day^{-1}.

The relationships between GPP_{VPM} and GPP_{EC} for individual crop types were evaluated through simple linear regression models (Fig. 10). For irrigated and rainfed maize, both $GPP_{VPM(EC)}$ and $GPP_{VPM(adjNARR)}$ agreed well with GPP_{EC}; but $GPP_{VPM(NARR)}$ was overestimated due to the positive bias of R_{NARR} (Fig. 10a and b). $GPP_{VPM(EC)}$ accounted for 89% of the variations of GPP_{EC}. $GPP_{VPM(NARR)}$ was also correlated well with GPP_{EC}, but it was overestimated by 18.4% and 29.6% for irrigated and rainfed maize, respectively. After adjusting R_{NARR}, α, RE, and RMSE for $GPP_{VPM(adjNARR)}$ were close to those of $GPP_{VPM(EC)}$. For irrigated and rainfed soybean, $GPP_{VPM(EC)}$ and $GPP_{VPM(adjNARR)}$ estimated GPP reasonably well with an underestimation less than −10% (Fig. 10c and d). $GPP_{VPM(NARR)}$ over-predicted GPP_{EC} by ~13% for irrigated and rainfed soybean.

The relationships between GPP_{VPM} and GPP_{EC} were further evaluated for maize through individual crop-sites and individual site-years (Fig. 11a, b, and Table 3). $GPP_{VPM(EC)}$ and $GPP_{VPM(adjNARR)}$ showed reliable GPP estimates for the irrigated and rainfed maize across the sites (Fig. 11a and b). Most sites had similar patterns and amplitudes of variability between $GPP_{VPM(EC)}$ and GPP_{EC} ($1 < \bar{\sigma}_{ratio} < 1.05$ and $0.95 < \rho < 0.98$, Fig. 11a) with low annual mean RMSEs (ca. 1.5–2.4 g C m^{-2} day^{-1}, Table 3). $GPP_{VPM(EC)}$ at RO1 and Bo1 didn't appear to adequately capture the amplitudes of variability of GPP_{EC} ($\bar{\sigma}_{ratio} = 0.7$ and 1.3) as indicated by relatively low ρ (0.92 and 0.82) and high RMSE (3.2 g C m^{-2} day^{-1} and 4.9 g C m^{-2} day^{-1}). The discrepancies were due to the underestimation of $GPP_{VPM(EC)}$ during the peak growing season at RO1 and the significant overestimation of $GPP_{VPM(EC)}$ after the peak growing season at Bo1 (Fig. 9). $GPP_{VPM(NARR)}$ simulated the phasing and timing of GPP_{EC} well (ρ was ca. 0.93–0.98). The RMSE of $GPP_{VPM(NARR)}$ (ca. 4.2–6.4 g C m^{-2} day^{-1}) was significantly higher than that of $GPP_{VPM(EC)}$ at most sites, indicating an overestimation caused the NARR. The adjustment of R_{NARR} resulted in similar patterns of $GPP_{VPM(adjNARR)}$ and $GPP_{VPM(EC)}$ at all sites, with a slight increase of RMSE (ca. 1.6–3.1 g C m^{-2} day^{-1}, Fig 11b and Table 3).

The relationships between GPP_{VPM} and GPP_{EC} were also evaluated for soybean through individual crop-sites and individual site-years (Fig. 11c, 11d, and Table 3). $GPP_{VPM(EC)}$ and $GPP_{VPM(adjNARR)}$ matched GPP_{EC} reasonably well. The variability of $GPP_{VPM(EC)}$ was similar to that of GPP_{EC} ($0.83 < \rho < 0.93$, Fig. 11c). NE2 and RO1 had a good agreement between $GPP_{VPM(EC)}$ and GPP_{EC}, as $\bar{\sigma}_{ratio}$ was close to 1 showing a low RMSE (1.4–2.0 g C m^{-2} day^{-1}, Table 3). At other sites (NE3, IB1, and Bo1), $GPP_{VPM(EC)}$ underestimated the variability of GPP_{EC} ($0.85 < \bar{\sigma}_{ratio} < 0.9$, Fig. 11c) with a high RMSE (2.0–2.6 g C m^{-2} day^{-1}). $GPP_{VPM(NARR)}$ correlated well with GPP_{EC} ($0.9 < \rho < 0.94$). However, the $\bar{\sigma}_{ratio}$ of $GPP_{VPM(NARR)}$ was larger than that of $GPP_{VPM(EC)}$ caused by the positive bias of R_{NARR}. After adjusting the bias of R_{NARR}, $GPP_{VPM(adjNARR)}$ matched GPP_{EC} better than did $GPP_{VPM(NARR)}$ (Fig. 11d).

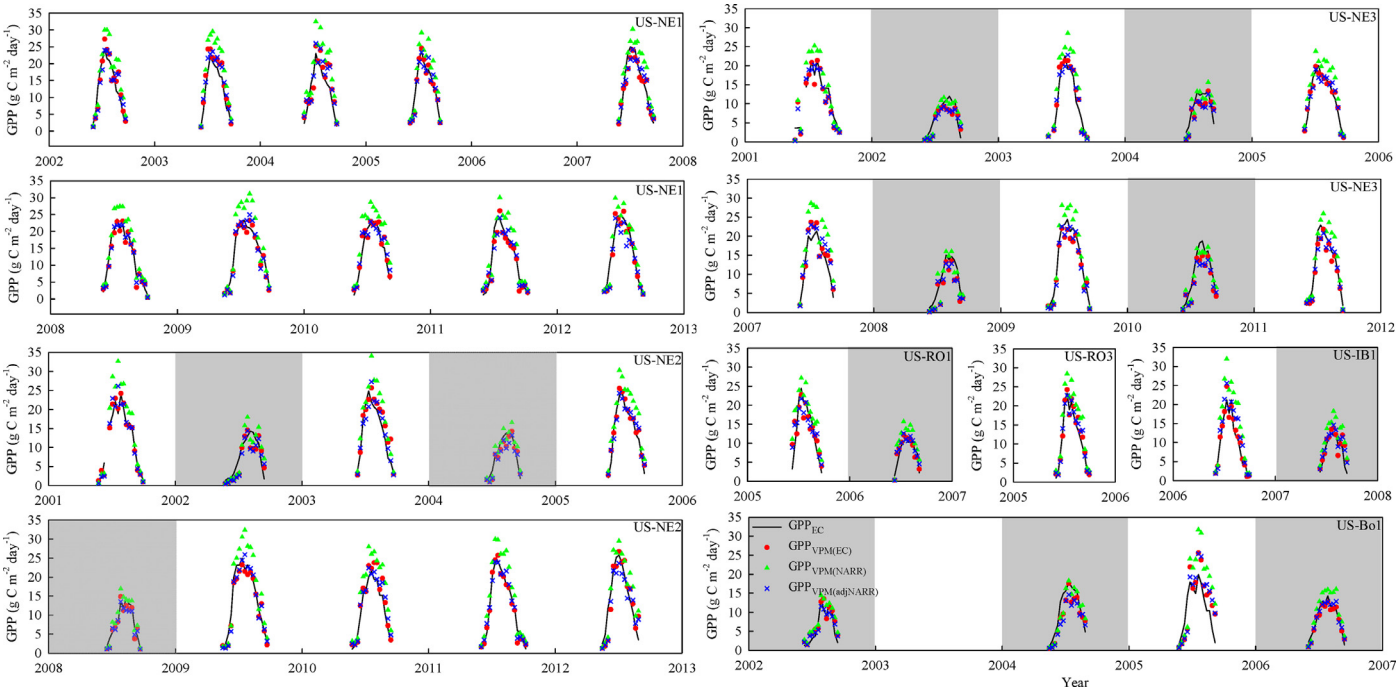

Fig. 9. Seasonal dynamics and interannual variations of GPP_{EC}, $GPP_{VPM(EC)}$, $GPP_{VPM(NARR)}$, and $GPP_{VPM(adjNARR)}$ for the crop site-years. The soybean site-years are highlighted.

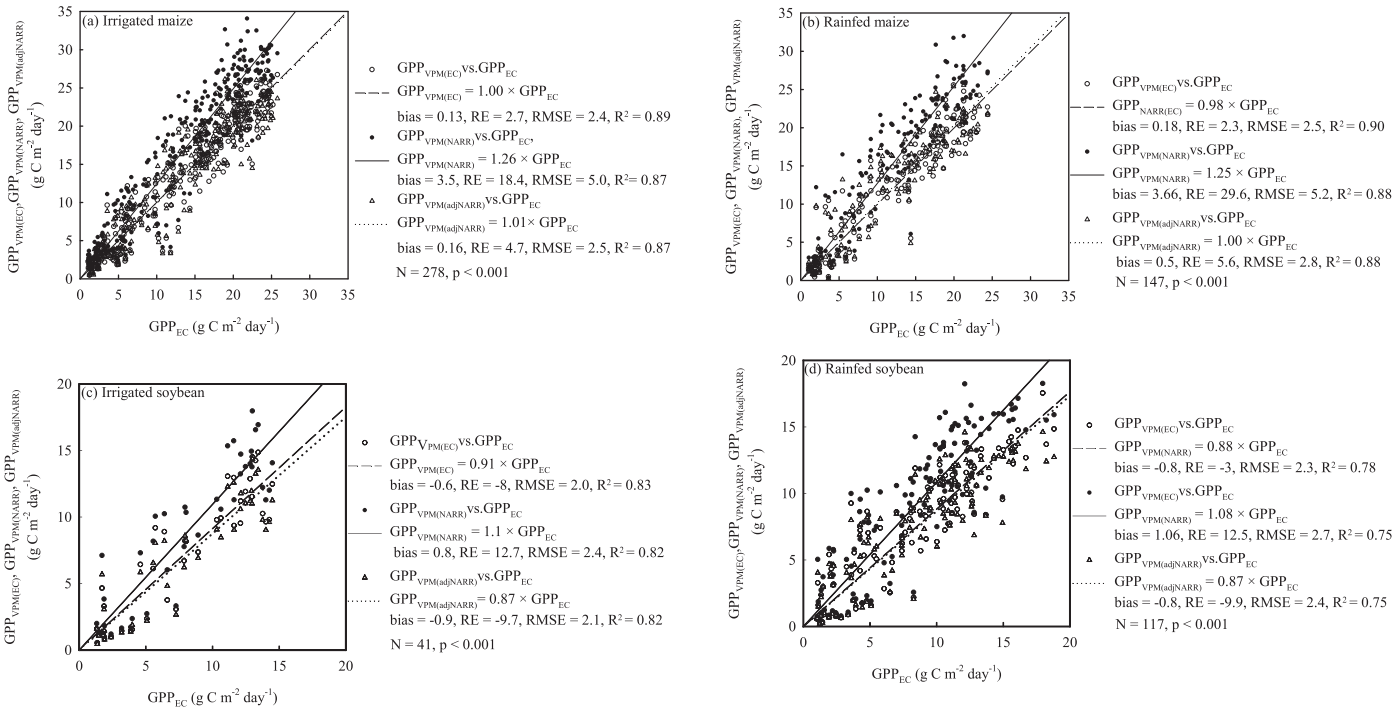

Fig. 10. Comparisons of $GPP_{VPM(EC)}$, $GPP_{VPM(NARR)}$, and $GPP_{VPM(adjNARR)}$ with GPP_{EC} for individual crop: (a) irrigated maize, (b) rainfed maize, (c) irrigates soybean, and (d) rainfed soybean.

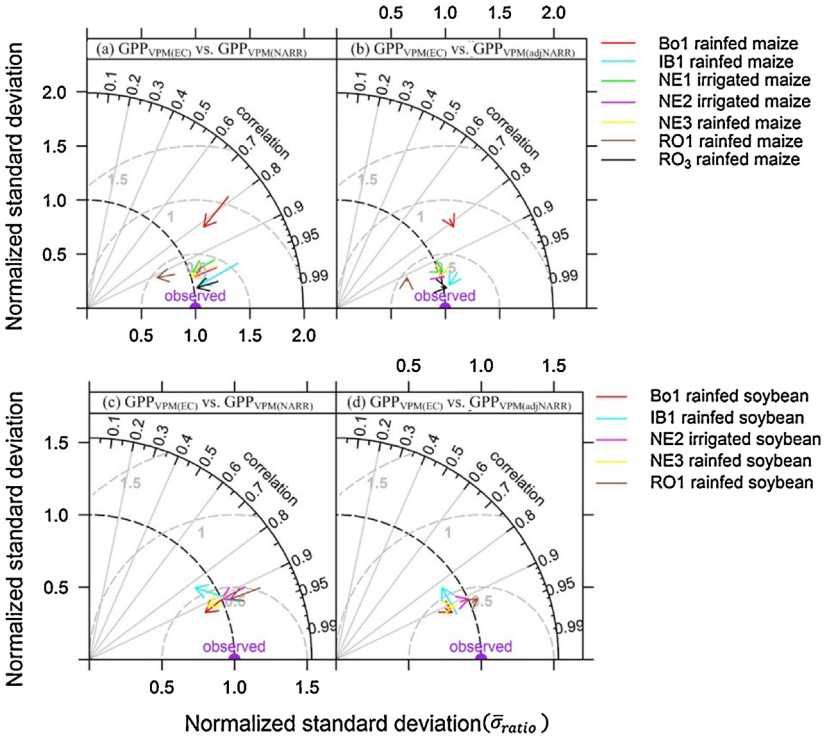

Fig. 11. Performances of the VPM driven by three climate datasets for individual crop-site: (a) and (b) $GPP_{VPM(EC)}$ vs. $GPP_{VPM(NARR)}$ and $GPP_{VPM(EC)}$ vs. $GPP_{VPM(adjNARR)}$ for the irrigated and rainfed maize; (c) and (d) $GPP_{VPM(EC)}$ vs. $GPP_{VPM(NARR)}$ and $GPP_{VPM(EC)}$ vs. $GPP_{VPM(adjNARR)}$ for the irrigated and rainfed soybean. The locations of the heads and tails of arrows quantify how GPP_{VPM} matches with GPP_{EC}, and the arrows show how the agreement of GPP_{VPM} with GPP_{EC} changes using different climate inputs. The distance to the origin is the ratio of the standard deviations of GPP_{VPM} and GPP_{EC} (Normalized standard deviation, $\bar{\sigma}_{ratio}$). The azimuthal angle is the correlation (ρ) showing the similarity of variation patterns between GPP_{VPM} and GPP_{EC}. The most ideal GPP_{VPM} estimate is the point "observed" with $\bar{\sigma}_{ratio} = 1$ and $\rho = 1$.

Table 3
A summary of the performances of the VPM driven by three sets of climate inputs at the crop sites.

Site ID	Crop type	$GPP_{VPM(EC)}$[a]			$GPP_{VPM(NARR)}$[b]			$GPP_{VPM(adjNARR)}$[c]		
		ρ	$\bar{\sigma}_{ratio}$	RMSE	ρ	$\bar{\sigma}_{ratio}$	RMSE	ρ	$\bar{\sigma}_{ratio}$	RMSE
US-NE1	Irrigated maize	0.95	1.03	2.4 ± 0.7	0.93	1.25	5.0 ± 1.1	0.93	1.00	2.7 ± 0.6
US-NE2	Irrigated maize	0.96	1.02	2.2 ± 0.8	0.95	1.24	4.8 ± 0.6	0.95	0.99	2.3 ± 0.6
	Irrigate soybean	0.91	1.00	2.0 ± 0.6	0.91	1.18	2.3 ± 0.7	0.90	0.94	2.0 ± 0.6
US-NE3	Rainfed maize	0.95	1.00	2.1 ± 0.5	0.95	1.26	4.2 ± 1.3	0.95	1.01	2.2 ± 0.5
	Rainfed soybean	0.91	0.89	2.6 ± 0.4	0.91	1.05	2.2 ± 0.3	0.90	0.84	2.8 ± 0.5
US-RO1	Rainfed maize	0.92	0.7	3.2	0.93	0.86	4.8	0.93	0.69	3.1
	Rainfed soybean	0.92	1.06	1.4	0.92	1.27	3.4	0.92	1.02	1.5
US-RO3	Rainfed maize	0.98	1.03	1.5	0.97	1.23	4.3	0.98	0.98	1.6
US-IB1	Rainfed maize	0.97	1.06	1.5	0.96	1.45	6.4	0.96	1.16	3.1
	Rainfed soybean	0.83	0.88	2.3	0.93	1.11	4.1	0.93	0.89	1.9
US-Bo1	Rainfed maize	0.82	1.31	4.9	0.78	1.66	8.6	0.78	1.33	5.5
	Rainfed soybean	0.93	0.86	2.0	0.91	1.03	2.5	0.91	0.83	2.3

[a–c]The VPM-based GPP estimates from in-situ, original and adjusted NARR climate data.

4. Discussion

4.1. Uncertainties of the NARR air temperature

T_{NARR} has been assumed to be relatively accurate in the studies of drought monitoring and the response of vegetation to climate change (Karnauskas et al., 2008; Karnieli et al., 2010; Wang et al., 2011). In this study, the 8-day T_{NARR} was mostly overestimated with a mean bias of 0.62 °C. This was consistent with the previous finding that T_{NARR} was biased warm at monthly intervals (Jiang and Yang, 2012). In general, the 8-day T_{NARR} agreed well with the in-situ observations across non-crop and crop site-years with the mean RMSE of 1.67 °C and 1.4 °C, respectively, showing relatively higher accuracy than other global reanalysis datasets (DAO, ECMWF, NCEP, MERRA) investigated by Zhao et al. (2006) and Decker et al. (2012).

4.2. Uncertainties of the NARR downward shortwave radiation

This study made an assumption that R_{EC} were ground truth. However, the errors or uncertainties associated with in-situ radiation observations also contributed to the differences between R_{NARR} and R_{EC}. R_{EC} at the AmeriFlux is measured by different pyranometers. The errors from pyranometers including instrument deployment and maintenance (leveling and shading) and sensor response errors such as thermal offset (Bush et al., 2000; Reda et al., 2005) determined the errors of R_{EC}. The errors of R_{EC} are subtle compared with the R_{NARR} biases, but one should not neglect their impacts considering the significant decay of long-term sensor stability (Stanhill and Cohen, 2001).

A number of studies have evaluated the monthly R_{NARR} at individual sites. Walsh (2009) evaluated the monthly R_{NARR} at the Alaska Barrow site and found that it had a lower bias (2.6 MJ m^{-2} day^{-1}) than did NCEP/NCAR (3.7 MJ m^{-2} day^{-1}). Kennedy et al. (2011) concluded that the bias of monthly R_{NARR} varied with sky conditions at the Atmospheric Radiation Measurement Program (ARM) Southern Great Plain (SGP) site. Markovic et al. (2009) reported that a systematic bias of monthly R_{NARR} in summer (5.3 MJ m^{-2} day^{-1}) was larger than that in winter (2.5 MJ m^{-2} day^{-1}). These evaluations implied that R_{NARR} had a large span of positive biases. However, their results cannot represent the overall accuracy of R_{NARR} at continental scale using limited sites. A recent study did a large-scale assessment of monthly R_{NARR} using 24 FLUXNET sites showing that R_{NARR} exhibited a positive bias of 3.2 MJ m^{-2} day^{-1} (Zhao et al., 2013a). The ideal temporal interval of climatic drivers for ecological models should be finer, i.e. hourly, daily, or weekly intervals, to demonstrate the diurnal or seasonal dynamics of carbon and energy fluxes (Abatzoglou, 2013; Huntzinger et al., 2013; Wei et al., 2013). Thus, we evaluated the accuracy of R_{NARR} at 8-day intervals and regional scale using all available AmeriFlux sites. The 8-day R_{NARR} well represented the seasonal dynamics of 8-day R_{EC}. Similar to monthly R_{NARR}, the bias of the 8-day R_{NARR} was positive and systematic with a large range across the U.S. The systematic overestimation of R_{NARR} is mainly caused by the insufficient simulation of light extinction caused by clouds, aerosols, and water vapor in the radiative transferring models (Kennedy et al., 2011; Markovic et al., 2009; Zhao et al., 2013a), and other topographical factors (i.e. elevation, slope, and aspect) (Schroeder et al., 2009; Zhao et al., 2013a).

Empirical or semi-empirical approaches are applied to correct the bias of R_{NARR}. The empirical approach develops the linear statistical regression model between the reanalysis and in-situ observations, then applies the model to other locations (Feng et al., 2007; Qian et al., 2006; Xiao et al., 2014). The empirical approach ignores the spatio-temporal variations in the R_{NARR} bias. Some studies developed the semi-empirical approach to account the impacts of clouds and topographical factors in the regression models (Schroeder et al., 2009; Zhao et al., 2013a). We followed the empirical approach to calibrate R_{NARR}, and meanwhile considered the spatial variation of regression models.

Simply estimating PAR as a constant ratio of R_{NARR} can introduce uncertainties to PAR. Theoretically, the band range of downward shortwave radiation (0.3–2.8 μm) does not match that of PAR (0.4–0.7 μm) (Sakamoto et al., 2011). Moreover, the ratio of PAR to downward shortwave radiation is not constant, as it temporally changes with the local weather condition (Gonzalez and Calbo, 2002; Jacovides et al., 2004; Papaioannou et al., 1993). Surface PAR datasets, such as the satellite-derived Global Land Surface Satellite (GLASS), might be an alternative PAR input for the regional and global ecological modeling (Cai et al., 2014; Eck and Dye, 1991; Frouin and Pinker, 1995; Jin et al., 2013; Pinker et al., 2010; Rubio et al., 2005; Zhao et al., 2013b).

4.3. Sensitivity of PEMs to various climate inputs

All analyses about the sensitivity of PEMs to climate inputs were focused on the PEM of the standard MODIS GPP product – the MODIS-PSN (Heinsch et al., 2006; Zhang et al., 2007; Zhao et al., 2006). These studies found that radiation, air temperature, and vapor pressure deficit (VPD) of the global reanalysis data were largely biased, and introduced significant errors to the standard MODIS GPP product. For instance, Zhao et al. (2006) found that the MODIS GPP showed significant differences when driven by DAO, NCAR, and ECMWF (>20 Pg Cyr^{-1}). Heinsch et al. (2006) collected 38 site-years of GPP_{EC} from 15 AmeriFlux sites to evaluate the accuracy of MODIS GPP driven by DAO and in-situ meteorology, and annual GPP derived from DAO was 23% higher than GPP_{EC} and

the RE of the GPP derived from DAO was much larger than that of the GPP derived from the in-situ meteorology. Note that these evaluations were conducted at monthly or longer intervals. Analyses on finer temporal scales such as weekly interval are needed in order to accurately evaluate the seasonal dynamics of the uncertainties of PEMs to climate data. Thus, we focused on quantifying the uncertainties of GPP_{VPM} to in-situ and NARR climate data at 8-day interval. The 8-day GPP_{VPM} driven by the in-situ meteorology, original and adjusted NARR data traced over 83–98% of GPP_{EC} variations for individual site-years, confirming their capabilities to simulate the response of crop photosynthesis to the environment change (i.e. light, temperature, and water), and tracked the phenological phases well (i.e. leaf-on and leaf-off stages). Similar to the MODIS-PSN, climate inputs had a strong impact on the VPM for cropland GPP estimates. $GPP_{VPM(EC)}$ well estimated GPP_{EC} for individual crops, sites, and site-years. $GPP_{VPM(NARR)}$ significantly overestimated GPP_{EC} as R_{NARR} was positively biased. This study addressed two climate inputs of air temperature and downward shortwave radiation for the VPM. The accuracies of other climate variables (VPD, precipitation, etc.) in reanalysis products might be more variable (Decker et al., 2012). Therefore, more uncertainties might be introduced to the PEMs that are driven by multiple climate variables.

4.4. Challenges in comparing GPP_{VPM} with GPP_{EC}

In one study like ours using GPP_{EC} to validate or constrain the GPP estimates from PEMs, two assumptions are often made: (1) GPP_{EC} is assumed to be accurate as the ground truth and (2) the eddy flux tower footprint is approximately equivalent to the image pixel. The uncertainties associated with these two assumptions, however, can contribute to the discrepancies between the PEM-based GPP estimates (GPP_{VPM} in this study) and GPP_{EC}.

There are a number of errors or uncertainties (random and systematic) from eddy covariance measurements. Random errors are attributed to the stochastic nature of turbulence, sampling errors, instrument system, and variations in the flux footprint (Richardson et al., 2012). Systematic errors arise from the combination of the unmet underlying theoretical assumptions, instrument calibration, and data processing techniques (Falge et al., 2001; Papale et al., 2006; Richardson et al., 2012). Furthermore, the eddy covariance provides direct measurement of NEE and GPP_{EC} is estimated as the difference between NEE and ecosystem respiration (R_{eco}) using flux-partitioning approaches, which may also introduce large uncertainties in GPP_{EC} (Desai et al., 2008; Reichstein et al., 2005; Stoy et al., 2006). For example, Desai et al. (2008) found annual GPP_{EC} varied $\sim$100 g C m^{-2} $year^{-1}$ among 23 partitioning methods. Thus, more efforts are needed to improve partitioning NEE into its gross components to help validate GPP in PEMs and other land surface models (Baldocchi et al., 2015).

The second assumption is questionable in heterogeneous landscapes. Limited by data availability, most PEMs are performed on 1 km spatial resolution of satellite images and might not represent the crop fields that towers are located in due to the mixed signals from other sub-pixel components. In this study, an in-situ landscape analysis showed that the heterogeneity of 500 m MODIS pixels was much improved over that of 1 km MODIS pixels at seven crop sites (Fig. S1). 500 m MODIS pixels were mainly covered by the crop fields that the towers measured except US-RO3 and US-Bo1. Even though the uncertainties of the GPP comparison caused by heterogeneous landscapes were diminished to some extent using the 500 m MODIS data in this study, further evaluations using high resolution images along with the downscaling techniques are required for implementing PEMs, especially at heterogeneous landscapes.

5. Conclusion

This study evaluated the uncertainties of the NARR surface meteorology and quantified the sensitivity of the VPM to the in-situ and NARR climate inputs at seven AmeriFlux crop eddy flux sites. Our results indicated that the bias of NARR resulted in considerable uncertainties in cropland GPP estimates. The 8-day NARR air temperature matched well with in-situ observations, but the NARR downward shortwave radiation showed large positive bias and led to the overestimation of GPP_{VPM}. An empirical correction of the NARR radiation improved the model performance.

The findings of this study confirm the good performance of the VPM on estimating maize and soybean GPP as long as meteorological inputs are accurate, and imply that the capability of the satellite-based PEMs for regional productivity monitoring at heterogeneous landscapes would be enhanced if the radiation of the regional reanalysis product can be improved to resolve the impacts of cloud cover and terrain. The proposed method to correct NARR radiation is limited to the crop sites in this study, and might not be applicable for other regions due to the large spatial variations of the NARR radiation bias. In addition to the meteorological data, further research is required to address the uncertainties of the PEM-based GPP estimates caused by other model inputs such as satellite data.

Acknowledgements

This study was supported by the National Institute of Food and Agriculture, U.S. Department of Agriculture, under award number 2013-69002-23146, and a research grant from the National Science Foundation EPSCoR program (Project No. IIA-1301789). We would like to thank Drs. Andrew E. Suyker, John Baker, Tilden Meyers, Roser Matamala for providing eddy flux data.

Appendix A. Supplementary data

Supplementary data associated with this article can be found, in the online version, at http://dx.doi.org/10.1016/j.agrformet.2015.07.003

References

Abatzoglou, J.T., 2013. Development of gridded surface meteorological data for ecological applications and modelling. Int. J. Climatol. 33 (1), 121–131.
Babst, F., Mueller, R.W., Hollmarm, R., 2008. Verification of NCEP reanalysis shortwave radiation with mesoscale remote sensing data. IEEE Geosci. Remote Sens. Lett. 5 (1), 34–37.
Baldocchi, D., et al., 2001. FLUXNET: a new tool to study the temporal and spatial variability of ecosystem-scale carbon dioxide, water vapor, and energy flux densities. Bull. Am. Meteorol. Soc. 82 (11), 2415–2434.
Baldocchi, D., Sturtevant, C., Contributors, F., 2015. Does day and night sampling reduce spurious correlation between canopy photosynthesis and ecosystem respiration? Agric. Forest Meteorol. 207 (0), 117–126.
Bush, B.C., Valero, F.P.J., Simpson, A.S., Bignone, L., 2000. Characterization of thermal effects in pyranometers: a data correction algorithm for improved measurement of surface insolation. J. Atmos. Ocean Technol. 17 (2), 165–175.
Cai, W.W., et al., 2014. Improved estimations of gross primary production using satellite-derived photosynthetically active radiation. J. Geophys. Res. Biogeosci. 119 (1), 110–123.
Chen, J.M., Liu, J., Cihlar, J., Goulden, M.L., 1999. Daily canopy photosynthesis model through temporal and spatial scaling for remote sensing applications. Ecol. Model. 124 (2–3), 99–119.
Chen, T., van der Werf, G.R., Gobron, N., Moors, E.J., Dolman, A.J., 2014. Global cropland monthly gross primary production in the year 2000. Biogeosciences 11 (14), 3871–3880.
Decker, M., et al., 2012. Evaluation of the reanalysis products from GSFC, NCEP, and ECMWF using flux tower observations. J. Clim. 25 (6), 1916–1944.
Desai, A.R., et al., 2008. Cross-site evaluation of eddy covariance GPP and RE decomposition techniques. Agric. Forest Meteorol. 148 (6–7), 821–838.
Dong, J., et al., 2015. Comparison of four EVI-based models for estimating gross primary production of maize and soybean croplands and tallgrass prairie under severe drought. Remote Sens. Environ. 162, 154–168.
Eck, T.F., Dye, D.G., 1991. Satellite estimation of incident photosynthetically active radiation using ultraviolet reflectance. Remote Sens. Environ. 38 (2), 135–146.

Falge, E., et al., 2001. Gap filling strategies for defensible annual sums of net ecosystem exchange. Agric. Forest Meteorol. 107 (1), 43–69.
Feng, X., et al., 2007. Net primary productivity of China's terrestrial ecosystems from a process model driven by remote sensing. J. Environ. Manag. 85 (3), 563–573.
Frouin, R., Pinker, R.T., 1995. Estimating photosynthetically active radiation (Par) at the earths surface from satellite-observations. Remote Sens. Environ. 51 (1), 98–107.
Gitelson, A.A., et al., 2006. Relationship between gross primary production and chlorophyll content in crops: implications for the synoptic monitoring of vegetation productivity. J. Geophys. Res. Atmos. 111 (D8).
Gleckler, P.J., Taylor, K.E., Doutriaux, C., 2008. Performance metrics for climate models. J. Geophys. Res. Atmos. 113 (D6).
Gonzalez, J.A., Calbo, J., 2002. Modelled and measured ratio of PAR to global radiation under cloudless skies. Agric. Forest Meteorol. 110 (4), 319–325.
Griffis, T.J., Baker, J.M., Zhang, J., 2005. Seasonal dynamics and partitioning of isotopic CO_2 exchange in C-3/C-4 managed ecosystem. Agric. Forest Meteorol. 132 (1–2), 1–19.
Guanter, L., et al., 2014. Global and time-resolved monitoring of crop photosynthesis with chlorophyll fluorescence. Proc. Natl. Acad. Sci. U. S. A. 111 (14), E1327–E1333.
Gupta, H.V., Kling, H., Yilmaz, K.K., Martinez, G.F., 2009. Decomposition of the mean squared error and NSE performance criteria: implications for improving hydrological modelling. J. Hydrol. 377 (1–2), 80–91.
Haberl, H., et al., 2007. Quantifying and mapping the human appropriation of net primary production in earth's terrestrial ecosystems. Proc. Natl. Acad. Sci. U. S. A. 104 (31), 12942–12945.
He, M., et al., 2013. Development of a two-leaf light use efficiency model for improving the calculation of terrestrial gross primary productivity. Agric. Forest Meteorol. 173 (0), 28–39.
Heinsch, F.A., et al., 2006. Evaluation of remote sensing based terrestrial productivity from MODIS using regional tower eddy flux network observations. IEEE Trans. Geosci. Remote Sens. 44 (7), 1908–1925.
Huntzinger, D.N., et al., 2013. The North American carbon program multi-scale synthesis and terrestrial model intercomparison project – Part 1: Overview and experimental design. Geosci. Model Dev. 6 (6), 2121–2133.
Jacovides, C.P., Timvios, F.S., Papaioannou, G., Asimakopoulos, D.N., Theofilou, C.M., 2004. Ratio of PAR to broadband solar radiation measured in Cyprus. Agric. Forest Meteorol. 121 (3–4), 135–140.
Jiang, X.Y., Yang, Z.L., 2012. Projected changes of temperature and precipitation in Texas from downscaled global climate models. Clim. Res. 53 (3), 229–244.
Jin, H.A., et al., 2013. Validation of global land surface satellite (GLASS) downward shortwave radiation product in the rugged surface. J. Mt. Sci. Engl. 10 (5), 812–823.
Kalfas, J.L., Xiao, X.M., Vanegas, D.X., Verma, S.B., Suyker, A.E., 2011. Modeling gross primary production of irrigated and rain-fed maize using MODIS imagery and CO_2 flux tower data. Agric. Forest Meteorol. 151 (12), 1514–1528.
Karnauskas, K.B., Ruiz-Barradas, A., Nigam, S., Busalacchi, A.J., 2008. North American droughts in ERA-40 global and NCEP North American Regional Reanalyses: a palmer drought severity index perspective. J. Clim. 21 (10), 2102–2123.
Karnieli, A., et al., 2010. Use of NDVI and land surface temperature for drought assessment: merits and limitations. J. Clim. 23 (3), 618–633.
Kennedy, A., Dong, X.Q., Xi, B.K., 2011. A comparison of MERRA and NARR reanalyses with the DOE ARM SGP data. J. Clim. 24 (17), 4541–4557.
Landis, D.A., Gardiner, M.M., van der Werf, W., Swinton, S.M., 2008. Increasing corn for biofuel production reduces biocontrol services in agricultural landscapes. Proc. Natl. Acad. Sci. U. S. A. 105 (51), 20552–20557.
Lobell, D.B., Asner, G.P., 2003. Climate and management contributions to recent trends in U.S. Agric. Yields Sci. 299 (5609), 1032.
Markovic, M., Jones, C.G., Winger, K., Paquin, D., 2009. The surface radiation budget over North America: gridded data assessment and evaluation of regional climate models. Int. J. Climatol. 29 (15), 2226–2240.
Mesinger, F., et al., 2006. North American regional reanalysis. Bull. Am. Meteorol. Soc. 87 (3), 343–360.
Meyers, T.P., Hollinger, S.E., 2004. An assessment of storage terms in the surface energy balance of maize and soybean. Agric. Forest Meteorol. 125 (1–2), 105–115.
Monteith, J.L., 1972. Solar-radiation and productivity in tropical ecosystems. J. Appl. Ecol. 9 (3), 747–766.
Monteith, J.L., Moss, C.J., 1977. Climate and the efficiency of crop production in Britain [and discussion]. Philos. Trans. R. Soc. B: Biol. Sci. 281, 277–294.
Papaioannou, G., Papanikolaou, N., Retalis, D., 1993. Relationships of photosynthetically active radiation and shortwave irradiance. Theor. Appl. Climatol. 48 (1), 23–27.
Papale, D., et al., 2006. Towards a standardized processing of Net Ecosystem Exchange measured with eddy covariance technique: algorithms and uncertainty estimation. Biogeosciences 3 (4), 571–583.
Peng, Y., Gitelson, A.A., 2011. Application of chlorophyll-related vegetation indices for remote estimation of maize productivity. Agric. Forest Meteorol. 151 (9), 1267–1276.
Peng, Y., Gitelson, A.A., 2012. Remote estimation of gross primary productivity in soybean and maize based on total crop chlorophyll content. Remote Sens. Environ. 117, 440–448.
Peng, Y., Gitelson, A.A., Keydan, G., Rundquist, D.C., Moses, W., 2011. Remote estimation of gross primary production in maize and support for a new paradigm based on total crop chlorophyll content. Remote Sens. Environ. 115 (4), 978–989.
Pinker, R.T., Zhao, M.S., Wang, H.M., Wood, E.F., 2010. Impact of satellite based PAR on estimates of terrestrial net primary productivity. Int. J. Remote Sens. 31 (19), 5221–5237.
Prince, S.D., Goward, S.N., 1995. Global primary production: a remote sensing approach. J. Biogeogr. 22 (4–5), 815–835.
Qian, T.T., Dai, A., Trenberth, K.E., Oleson, K.W., 2006. Simulation of global land surface conditions from 1948 to 2004. Part I: Forcing data and evaluations. J. Hydrometeorol. 7 (5), 953–975.
Raich, J.W., et al., 1991. Potential net primary productivity in South-America – application of a global-model. Ecol. Appl. 1 (4), 399–429.
Ramankutty, N., Evan, A.T., Monfreda, C., Foley, J.A., 2008. Farming the planet: 1. Geographic distribution of global agricultural lands in the year 2000. Global Biogeochem. Cycle 22 (1), GB1003.
Reda, I., et al., 2005. Using a blackbody to calculate net longwave responsivity of shortwave solar pyranometers to correct for their thermal offset error during outdoor calibration using the component sum method. J. Atmos. Ocean Technol. 22 (10), 1531–1540.
Reichstein, M., et al., 2005. On the separation of net ecosystem exchange into assimilation and ecosystem respiration: review and improved algorithm. Global Change Biol. 11 (9), 1424–1439.
Richardson, A., et al., 2012. Uncertainty quantification. In: Aubinet, M., Vesala, T., Papale, D. (Eds.), Eddy Covariance. Springer Atmospheric Sciences. Springer, Netherlands, pp. 173–209.
Rubio, M.A., Lopez, G., Tovar, J., Pozo, D., Batlles, F.J., 2005. The use of satellite measurements to estimate photosynthetically active radiation. Phys. Chem. Earth 30 (1–3), 159–164.
Running, S., Thornton, P., Nemani, R., Glassy, J., 2000. Global terrestrial gross and net primary productivity from the earth observing system. In: Sala, O., Jackson, R., Mooney, H., Howarth, R. (Eds.), Methods in Ecosystem Science. Springer, New York, pp. 44–57.
Running, S.W., et al., 2004. A continuous satellite-derived measure of global terrestrial primary production. Bioscience 54 (6), 547–560.
Sakamoto, T., Gitelson, A.A., Wardlow, B.D., Verma, S.B., Suyker, A.E., 2011. Estimating daily gross primary production of maize based only on MODIS WDRVI and shortwave radiation data. Remote Sens. Environ. 115 (12), 3091–3101.
Schroeder, T.A., Hember, R., Coops, N.C., Liang, S.L., 2009. Validation of solar radiation surfaces from MODIS and reanalysis data over topographically complex terrain. J. Appl. Meteorol. Clim. 48 (12), 2441–2458.
Stanhill, G., Cohen, S., 2001. Global dimming: a review of the evidence for a widespread and significant reduction in global radiation with discussion of its probable causes and possible agricultural consequences. Agric. Forest Meteorol. 107 (4), 255–278.
Stoy, P.C., et al., 2006. An evaluation of models for partitioning eddy covariance-measured net ecosystem exchange into photosynthesis and respiration. Agric. Forest Meteorol. 141 (1), 2–18.
Taylor, K.E., 2001. Summarizing multiple aspects of model performance in a single diagram. J. Geophys. Res. Atmos. 106 (D7), 7183–7192.
Troy, T.J., Wood, E.F., 2009. Comparison and evaluation of gridded radiation products across northern Eurasia. Environ. Res. Lett. 4 (4).
Verma, S.B., et al., 2005. Annual carbon dioxide exchange in irrigated and rainfed maize-based agroecosystems. Agric. Forest Meteorol. 131 (1–2), 77–96.
Veroustraete, F., Sabbe, H., Eerens, H., 2002. Estimation of carbon mass fluxes over Europe using the C-Fix model and Euroflux data. Remote Sens. Environ. 83 (3), 376–399.
Wagle, P., Xiao, X.M., Suyker, A.E., 2015. Estimation and analysis of gross primary production of soybean under various management practices and drought conditions. ISPRS J. Photogramm. 99, 70–83.
Walsh, J.E., 2009. Arctic cloud fraction and radiative fluxes in atmospheric reanalyses. J. Clim. 22 (9), 2316–2334.
Wang, X.H., et al., 2011. Spring temperature change and its implication in the change of vegetation growth in North America from 1982 to 2006. Proc. Natl. Acad. Sci. U. S. A. 108 (4), 1240–1245.
Wei, Y., et al., 2013. The North American carbon program multi-scale synthesis and terrestrial model intercomparison project – Part 2: Environmental driver data. Geosci. Model Dev. Discuss. 6 (4), 5375–5422.
Wheeler, T., von Braun, J., 2013. Climate change impacts on global food security. Science 341 (6145), 508–513.
Wu, C.Y., et al., 2009. Remote estimation of gross primary production in wheat using chlorophyll-related vegetation indices. Agric. Forest Meteorol. 149 (6–7), 1015–1021.
Xiao, J., Davis, K.J., Urban, N.M., Keller, K., Saliendra, N.Z., 2011. Upscaling carbon fluxes from towers to the regional scale: influence of parameter variability and land cover representation on regional flux estimates. J. Geophys. Res. Biogeosci. 116 (G3), G00J06.
Xiao, J., et al., 2014. Data-driven diagnostics of terrestrial carbon dynamics over North America. Agric. Forest Meteorol. 197, 142–157.
Xiao, X.M., et al., 2004a. Satellite-based modeling of gross primary production in an evergreen needleleaf forest. Remote Sens. Environ. 89 (4), 519–534.
Xiao, X.M., et al., 2004b. Modeling gross primary production of temperate deciduous broadleaf forest using satellite images and climate data. Remote Sens. Environ. 91 (2), 256–270.

Yuan, W., et al., 2014. Global comparison of light use efficiency models for simulating terrestrial vegetation gross primary production based on the LaThuile database. Agric. Forest Meteorol. 192–193, 108–120.
Yuan, W.P., et al., 2010. Global estimates of evapotranspiration and gross primary production based on MODIS and global meteorology data. Remote Sens. Environ. 114 (7), 1416–1431.
Zhang, F., et al., 2012. Evaluating spatial and temporal patterns of MODIS GPP over the conterminous U.S. against flux measurements and a process model. Remote Sens. Environ. 124, 717–729.
Zhang, K., et al., 2007. Sensitivity of pan-Arctic terrestrial net primary productivity simulations to daily surface meteorology from NCEP-NCAR and ERA-40 reanalyses. J. Geophys. Res. Biogeosci. 112 (G1).
Zhang, Q.Y., et al., 2014. Estimation of crop gross primary production (GPP): I. Impact of MODIS observation footprint and impact of vegetation BRDF characteristics. Agric. Forest Meteorol. 191, 51–63.
Zhang, Q.Y., et al., 2015. Estimation of crop gross primary production (GPP): II. Do scaled MODIS vegetation indices improve performance? Agric. Forest Meteorol. 200, 1–8.
Zhao, L., Lee, X.H., Liu, S.D., 2013a. Correcting surface solar radiation of two data assimilation systems against FLUXNET observations in North America. J. Geophys. Res. Atmos. 118 (17), 9552–9564.
Zhao, M., Running, S.W., Nemani, R.R., 2006. Sensitivity of Moderate Resolution Imaging Spectroradiometer (MODIS) terrestrial primary production to the accuracy of meteorological reanalyses. J. Geophys. Res. Biogeosci. 111 (G1).
Zhao, X., et al., 2013b. The Global Land Surface Satellite (GLASS) remote sensing data processing system and products. Remote Sens. Basel 5 (5), 2436–2450.
Zib, B.J., Dong, X.Q., Xi, B.K., Kennedy, A., 2012. Evaluation and intercomparison of cloud fraction and radiative fluxes in recent reanalyses over the arctic using BSRN surface observations. J. Clim. 25 (7), 2291–2305.